Open Loop Nonlinear Optimal Tracking Control of a Magnetostrictive Terfenol-D Actuator

William S. Oates [1], Phillip G. Evans [2], Ralph C. Smith [3], and Marcelo J. Dapino [4]

Department of Mechanical Engineering[1]
Florida A&M/Florida State University
Tallahassee, FL 32310-6046

Department of Mechanical Engineering[2,4]
Ohio State University
Columbus, OH 43210

Center for Research in Scientific Computation[3]
Department of Mathematics
North Carolina State University
Raleigh, NC 27695

Abstract

A homogenized energy model was implemented in a model-based nonlinear control design to accurately track a reference displacement signal for high frequency magnetostrictive actuator applications. Rate dependent nonlinear and hysteretic magnetostrictive constitutive behavior is incorporated into the finite-dimensional optimal control design to improve control at high frequency. The integration of the rate-dependent nonlinear and hysteretic magnetostrictive constitutive model in the control design minimized the amount of feedback required for precision control. The control design is validated experimentally and shown to accurately track a reference signal at frequencies up to at least 1 kHz.

Keywords: Hysteresis, magnetostrictive, nonlinear control, optimal control, homogenization

1. Introduction

The integration of smart materials into structures and systems continues to be a critical component for enhancing the performance of many biomedical, automotive, aerospace, and industrial applications. The large forces, small displacements and broadband capability afforded by these materials are desirable characteristics that are useful many of these applications. Magnetostrictive materials are one example of smart materials which contain magnetic moments that reorient when a large magnetic field is applied. The magnetic field induces displacement and force and thus provides actuation for applications such as sonar arrays and high speed machining.

Although magnetostrictive materials have been successfully implemented in a number of applications, limitations associated with nonlinear and hysteretic material behavior have presented challenges in developing high performance actuation response over a broad frequency range. The nonlinear and hysteretic material behavior is primarily due to the reorientation of local magnetic variants that align with the applied magnetic fields. Moderate to large field levels can induce $\sim$0.1% strain in polycrystalline Terfenol-D and up to 6% strain in single crystal ferromagnetic shape memory alloys [1]; at these field levels, obtaining accurate and precise control is difficult due to the nonlinearities and magnetic hysteresis. This has motivated research in developing novel

[1]Email: woates@eng.fsu.edu, Telephone: (850) 410-6190
[2]Email: evans.895@osu.edu, Telephone: (614) 247-7480
[3]Email: rsmith@eos.ncsu.edu, Telephone: (919) 515-7552
[4]Email: dapino.1@osu.edu, Telephone: (614) 688-3689

control designs that can effectively compensate for nonlinearities induced by ferromagnetic switching to provide accurate forces or precision displacements over a broad frequency range.

We implement a model-based nonlinear control design where the constitutive law is directly incorporated into an optimal nonlinear control design. This approach is shown to improve tracking control accuracy for a magnetostrictive transducer at frequencies up to 1 kHz. Nonlinear control of magnetostrictive materials is not new and has been investigated by [2]; however, the model-based control design used a Preisach-based nonlinear inverse compensator to track a reference signal up to approximately 30 Hz. In the analysis presented here, comparisons between the nonlinear optimal control design and classical Proportional-Integral (PI) control are conducted. It is demonstrated that PI tracking control performance begins to degrade for sinusoidal reference displacements with frequencies at or above 500 Hz. The bandwidth of the actuator is improved by directly incorporating the constitutive behavior within the control design. Reasonable tracking control is achieved for frequencies up to at least 1 kHz.

The experimental analysis presented here employs a nonlinear control design previously analyzed numerically for controlling a magnetostrictive transducer operating in current control mode [3, 4]. In Section 2, the experimental set-up is described. In Section 3, the constitutive model and dynamic model are presented and compared to open loop actuator characterizations. In Section 4, the nonlinear control design is presented and compared to classic proportional-integral (PI) control to identify operating regimes where the nonlinear control design provides enhanced performance. Section 5 includes discussion and concluding remarks.

2. Experimental Implementation

An Etrema Products, Inc., magnetostrictive Terfenol-D actuator model MFR OTY77 was used in the control experiments. The actuator employs a Terfenol-D rod 12.5 mm in diameter by 100 mm in length which is subjected to a 10-14 MPa preload and ∼40 kA/m magnetic field bias from a permanent magnetic. The drive coil rating is 6.2 kA/m·A with a 3.4 A_{rms} limit. Figure 1 illustrates a schematic of the internal components in the actuator which includes a Terfenol-D rod, a compression bolt and Belleville washers to preload the rod, a surrounding wound wire solenoid and permanent magnet.

Voltage control is used to control the Terfenol-D actuator which is generated by a 16-bit digital-to-analog converter (DAC) on a dSPACE DS1104 controller board. The controller board output has a range of 10 V and >80 dB signal-to-noise ratio. A linear amplifier is used to obtain the necessary voltage gain to the wound wire solenoid in the Etrema motor. The amplifier gain is 17 V/V and the amplifier bandwidth is 20 kHz.

Reported data includes the DS1104 drive voltage, actuator current, and actuator strain. The current signal is sampled using the 16-bit analog-to-digital (ADC) on the DS1104 board. The strain measurement is simultaneously sampled with the same ADC from a Lion Precision capacitive sensor (PX405JTC probe with DMT10R driver) with a sensitivity of 2.5 m/V and bandwidth of 12.5 kHz. An Omega Engineering, Inc. signal amplifier model OMNI-AMP III DC with a gain of 10 V/V and a bandwidth of 10 kHz is used to match the dynamic

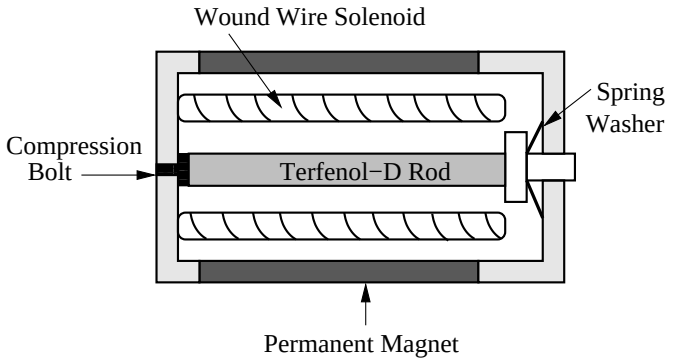

Figure 1: Schematic of the Terfenol-D actuator used in the control experiments.

range of the strain measurement with the range of the ADC.

3. Model Development

The nonlinear and hysteretic material modeling summarized here is based on a stochastic homogenized energy model which is based on previous work described in detail in [5–10]. Here, only key equations are given to motivate the implementation of the constitutive model in the structural dynamic model and control design.

The power amplifier employed in the control experiments uses voltage control; however, the homogenized energy model is formulated using an applied magnetic field. Therefore, the homogenized energy model was extended to relate voltage to current to simplify experimental implementation. Although a hardware modification could be done to implement current control, the modeling approach was chosen to reduce challenges associated with achieving robust current control over a broad frequency spectrum. This approach results in directly determining the nonlinear voltage control input from the homogenized energy model, structural dynamic relations and optimal control design.

The structural dynamics of the actuator is quantified using a lumped parameter model although a distributed weak PDE formulation can be employed to incorporate spatial dependence along the actuator length. The lumped parameter model is typically sufficient when the operating frequencies are below resonance and disturbances are negligible. For more general reference displacements and disturbance loads that excite higher order harmonics, a finite element model may be necessary. Finite element models can be directly incorporated into the model and control design as discussed in [3, 4, 10].

3.1 Rate-Dependent Ferromagnetic Homogenized Energy Model

An energy description at the mesoscopic length scale is employed to develop the homogenized energy at the macroscopic length scale. This local energy formulation is used to predict macroscopic constitutive behavior using a stochastic representation of material inhomogeneities relating the nucleation and growth of local ferromagnetic domains to macroscopic actuator displacements.

The Gibbs energy at the mesoscopic length scale is given for uni-axial loading

$$G(M,T) = \Psi(M,T) - \mu_0 H M \tag{1}$$

where $\Psi(M,T)$ is the Helmholtz energy detailed in [10], T is temperature, H is the magnetic field, and M is the magnetization. The one-dimensional Helmholtz energy function is a double-well potential below the Curie point T_c which gives rise to stable spontaneous magnetization with equal magnitude in the positive and negative directions.

The effects of rate-dependent hysteresis under applied fields are often present and must be included in the constitutive model. This effect is modeled using the Boltzmann relation

$$\mu(G) = Ce^{-GV/kT} \tag{2}$$

which quantifies the probability μ of achieving an energy density level G. Here kT/V is the relative thermal energy where V is a representative volume element at the mesoscopic length scale, k is Boltzmann's constant, and the constant C is specified to ensure integration to unity.

The Boltzmann relation gives rise to the *local* expected values

$$\langle M_+ \rangle = \int_{M_I}^{\infty} M\mu(G)dM \quad , \quad \langle M_- \rangle = \int_{-\infty}^{-M_I} M\mu(G)dM \tag{3}$$

of the magnetization associated with positively and negatively oriented dipoles, respectively. Here $\pm M_I$ are the positive and negative inflection points in the Helmholtz energy definition.

The local magnetization variants are defined by a volume fraction of variants x_+ and x_- having positive and negative orientations, respectively. The conservation relation $x_- + x_+ = 1$ must hold for the volume fraction of magnetization variants. The kinetic equations govern the evolution of variants that switch. The rate-dependent

behavior is determined by a set of transition likelihoods that define the probabilities that magnetization variants switch into negative or positive directions–more details can be found in [8–11].

The resulting local average magnetization is quantified by the relation

$$\overline{M} = x_+\langle M_+\rangle + x_-\langle M_-\rangle. \tag{4}$$

The macroscopic magnetization

$$[M(H)](t) = \int_{-\infty}^{\infty}\int_{0}^{\infty} \nu(H_c, H_I)\left[\overline{M}(H + H_I; H_c, \xi)\right](t) dH_I dH_c \tag{5}$$

is computed from the distribution of local variants from the relation where $\nu(H_c, H_I)$ denotes the distribution of coercive fields (H_c), interaction fields (H_I) and ξ represents the initial distribution of the local variants.

The densities can often be modeled as lognormal or normal distributions; however, when more accurate model predictions are critical such as in the case where precision control is desired, a general density can be fit to data. A general density is used in the present analysis and the values are determined by employing a parameter optimization technique to obtain sufficient model accuracy in predicting rate-dependent hysteresis. Details describing techniques to identify general densities can be found in [9, 10].

Once the macroscopic magnetization is quantified using (5), the forces generated by the magnetostrictive actuator must be quantified for implementation within the control design. This is provided by the constitutive law

$$\sigma = Y^M\varepsilon + c_D\dot{\varepsilon} - a_1(M(H) - M^r) - a_2(M(H) - M^r)^2 \tag{6}$$

representing uniaxial stress in the magnetostrictive actuator. The effective properties of the actuator include Y^M as the elastic modulus at constant magnetization, c_D as the Kelvin-Voigt damping parameter, ε as the linear strain component in the direction of loading, a_1 as the piezomagnetic coefficient and a_2 as the magnetostrictive coefficient. The time rate of change of the strain is denoted by $\dot{\varepsilon}$. The stress fields are assumed to be limited to the linear elastic regime where irreversible ferromagnetic switching is negligible. The magnetization $M(H)$ is computed using (5) where M^r is the initial macroscopic remanent state of the material. The material parameters associated with the homogenized energy model are given in Table 1. These parameters were identified from the experimental results presented in Section 3.4 using parameter optimization techniques detailed in [10].

3.2 Structural Model

The constitutive relations given by (5) and (6) are used to develop a system model that quantifies forces and displacements when a magnetic field or stress is applied to the magnetostrictive actuator. The partial differential equation (PDE) model is first given and then formulated as a lumped parameter ordinary differential equation (ODE). The effective stiffness, mass and damping factor are determined from the parameter optimization which is based on the structural dynamics of the Terfenol-D actuator and the damped oscillator used in preloading the actuator. A simple schematic of this configuration is illustrated in Figure 2.

A balance of forces gives

Table 1: Parameters employed in the homogenized energy model. χ_m is the magnetic susceptibility. A thermal energy parameter, $\gamma = \frac{V}{kT}$, has been used where k is Boltzmann's constant, V is a local representative volume element and T is the temperature. M^s is the local remanent magnetization and τ is the time constant; see [10] for details.

$\chi_m = 3.3$
$\gamma = 1.23 \times 10^8\ ms^2/kg$
$M^s = 190\ kA/m$
$\tau = 1.15 \times 10^{-4}\ s$

Table 2: Model parameters for the magnetostrictive actuator and damped oscillator. The parameter optimization identified the magnetostrictive coefficient a_2 to be zero for the operating regime considered.

$\overline{k} = 1.96 \times 10^7\ N/m$	$\overline{m} = .013\ kg$
$a_1 = 3275\ N/Am$	$\overline{c}_D = 2.3 \times 10^3\ Ns/m$
$a_2 = 0\ Nm^2/A^2$	$A = 1.27 \times 10^{-4}\ m^2$

$$\rho A \frac{\partial^2 w}{\partial t^2} = \frac{\partial N_{tot}}{\partial x} \tag{7}$$

where the density of the actuator is denoted by ρ, the cross-section area is A and the displacement is denoted by w; [10, 12]. The total force N_{tot} acting on the actuator is

$$N_{tot}(t,x) = Y^M A \frac{\partial w}{\partial x} + c_D A \frac{\partial^2 w}{\partial x \partial t} + F_m(H) \tag{8}$$

where the elastic restoring force is given by the first term on the right hand side of the equation and Kelvin-Voigt damping is incorporated in the second term. The model focuses on relative displacements from the preloaded reference state. The linear elastic strain component in the direction of loading is defined by $\varepsilon = \frac{\partial w}{\partial x}$. The coupling force F_m represents forces generated by the applied field where

$$F_m(H) = A[a_1(M(H) - M^r) + a_2(M(H) - M^r)^2] \tag{9}$$

and the hysteretic and nonlinear $H - M$ relation is specified by (5).

As illustrated in Figure 2, the boundary conditions are defined by a zero displacement at $x = 0$ and the balance of forces at $x = \ell$ yields

$$N_{tot}(t,\ell) = -k_L w(t,\ell) - c_L \frac{\partial w}{\partial t}(t,\ell) - m_L \frac{\partial^2 w}{\partial t^2}(t,\ell). \tag{10}$$

The initial conditions are $w(0,x) = 0$ and $\frac{\partial w}{\partial x}(0,x) = 0$.

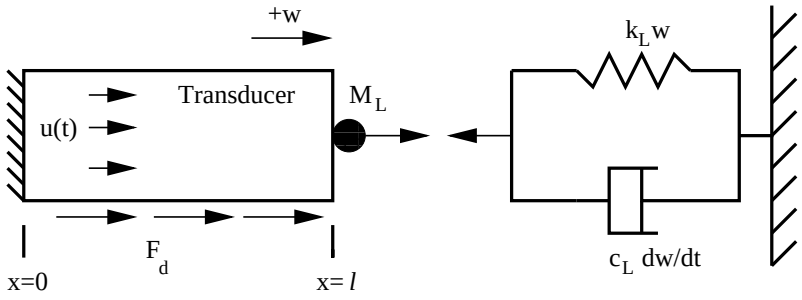

Figure 2: Magnetostrictive actuator with damped oscillator used to quantify loads under a time varying magnetic field. Disturbance forces along the actuator are given by F_d and the control input is $u(t)$.

3.2.1 Approximation Method

The second order differential equation given by (7) with boundary conditions (10) is rewritten in the form

$$\overline{m}\ddot{w} + \overline{c}_D\dot{w} + \overline{k}w = F_m(H) + F_d \tag{11}$$

where the effective mass $\overline{m} = \rho A\ell + m_L$, damping $\overline{c}_D = \frac{c_D A}{\ell} + c_L$ and stiffness $\overline{k} = \frac{Y^M A}{\ell} + k_L$ coefficients are given by the superposition of the Terfenol-D rod and the end damped oscillator.

Model parameters associated with the magnetostrictive actuator and damped oscillator used in the control design are given in Table 2.

For control implementation, (11) can be reformulated as a first order system

$$\begin{aligned} \dot{\mathbf{x}}(t) &= \mathbf{A}\mathbf{x}(t) + [\mathbf{B}(u)](t) \\ \mathbf{x}(0) &= \mathbf{x_0} \\ y(t) &= \mathbf{C}\mathbf{x}(t) \end{aligned} \tag{12}$$

where $\mathbf{x}(t) = [w, \dot{w}]^T$ includes actuator displacement and velocity at the tip of the actuator. The matrix $\mathbf{A}$ incorporates the mass, damping and stiffness matrices given in (11) and $[\mathbf{B}(u)](t)$ includes the nonlinear input where $u(t)$ is defined as the magnetic field. The initial conditions are defined by $\mathbf{x_0}$. The output of the system $y(t)$ is a function of the system states according to the matrix $\mathbf{C} = [1, 0]$ where only the displacement at the end of the actuator is measurable. The form of the state space model given by (12) can incorporate finite element nodal solutions; however, in the present case a lumped parameter model is used which is sufficient for the operating regime considered. For more general operating regimes that may include spatial variations in displacement along the rod, finite element formulations should be used, see [4, 10].

Predictions of the constitutive behavior at multiple frequencies using (12) is illustrated in Figure 3 and compared to experimental results. A reasonable estimation of rate-dependent hysteresis is achieved over the frequency range 100 Hz to 500 Hz using the parameters in Tables 1 and 2. However, voltage control is used in the control experiments; therefore, the model is extended to include nonlinear electrical impedance relations to obtain a model that can quantify the nonlinear voltage control input for experimental implementation.

3.3 Nonlinear Current-Voltage Relations

A nonlinear lumped-circuit model is used to relate the input voltage to the magnetic field applied to the Terfenol-D actuator. The lumped-circuit model consists of a linear amplified voltage input, electric resistance, and a nonlinear inductance associated with the Terfenol-D actuator. Key equations are given here to illustrate how the nonliear voltage control is used in the optimal control design; see [13] for more details.

The nonlinear inductance is quantified by coupling the homogenized energy model with the lumped-electric circuit model. The first-order nonlinear ODE for a resistor in series with a nonlinear inductor is

$$\begin{aligned} L(M)\frac{di(t)}{dt} + Ri(t) &= V(t) \\ i(0) &= i_0 \end{aligned} \tag{13}$$

where $L(M)$ is the inductance written as a function of magnetization, i is the current, V is the voltage input, R is the resistance and the initial conditions are defined by i_0.

The magnetic field H applied to the Terfenol-D rod is related to the current by the relation

$$H = \frac{N}{\ell}i \tag{14}$$

where ℓ is the actuator length and N is the number of coils in the solenoid. Here, the tangential magnetic field on the surface of the Terfenol-D rod is assumed to fully penetrate the rod cross-section area over the frequency range considered. This assumes the effects of eddy current losses are negligible.

The inductance can be related to the magnetic permeability and the wound wire solenoid. From classic electromagnetics [14], the inductance describes the self-induced emf which is proportional to the time rate of change of current. The inductance can therefore be written as

$$L(M) = \frac{N^2}{\ell} \frac{d\Phi_m(M)}{dH} \tag{15}$$

where N is the number of turns in the solenoid and Φ_m is the flux. Since eddy currents in the Terfenol-D actuator have been neglected and if rod end effects are neglected, the flux can be defined by

$$\Phi_m = BA \tag{16}$$

for the induction component B parallel to the rod length and A is the cross sectional area.

The nonlinear inductance can be determined by including changes in the remanent magnetization with respect to the change in field given in (15). This can be described by representing the magnetization as a superposition of a linear term and the rate-dependent nonlinear and hysteretic term associated with the change in remanent magnetization. This is considered at the macroscopic length scale by writing (5) as

$$[M(H)](t) = \chi_m H(t) + [M^r(H)](t) \tag{17}$$

where $\chi_m = \mu_0(1 + \chi_m)$ is the macroscopic magnetic susceptibility and $M^r(H)$ is the remanent magnetization. The induction relation $B = \mu_0(H + M)$ can then be written as

$$[B(H)](t) = \mu_0(1 + \chi_m)H(t) + \mu_0 [M^r(H)](t) \tag{18}$$

where $\mu_0 = 4\pi \times 10^{-7}$ Wb/Am is the permeability of free space.

The nonlinear induction is then

$$L(M) = \frac{N^2 A}{\ell} \frac{dB}{dH} = \frac{N^2 A}{\ell} \left(\mu_m + \mu_o \frac{dM^r}{dH} \right) \tag{19}$$

where μ_m is the relative permeability of the material. Note that this relation simplifies to the classic linear inductance relation for a wound wire solenoid when the remanent magnetization is constant. Whereas this approach is expected to provide a relation for nonlinear inductance, $H - B$ data is not available from the Terfenol-D actuator which requires estimating the inductance. A fitting parameter is introduced according to

$$L(M) = N \frac{dB}{di} \simeq K_L \frac{dy}{di} \tag{20}$$

where y is the Terfenol-D actuator displacement determined from (12) and K_L is quantified from the experimental results using voltage vs. current data and current vs. strain data. K_L was quantified at 100 Hz. The value that was quantified from the experiments was $K_L = 2 \times 10^5$ Vs/m which was used in the model and control design.

3.4 Actuator Characterization

Characterization of the actuator was done using open loop sinusoidal drive voltages at 100, 200, 300 and 500 Hz. Each data set was initiated by a half-cycle of a 1 Hz sine wave with an amplitude of 1 V to the amplifier-actuator system; this corresponds to a current of 4.6 A. After the initial magnetization half-cycle, sinusoidal voltage signals at frequencies 100, 200, 300, and 500 Hz were used to drive the Terfenol-D actuator. The peak-to-peak sinusoidal voltage inputs were adjusted to achieve minor loops extending 60 μm. Strain-current minor loops are illustrated in Figure 3 for the frequencies 100 and 500 Hz, additional experimental results are given in [13]. The data given in these figures are compared to model predictions using the homogenized energy model and lumped electric circuit model discussed in the previous sections.

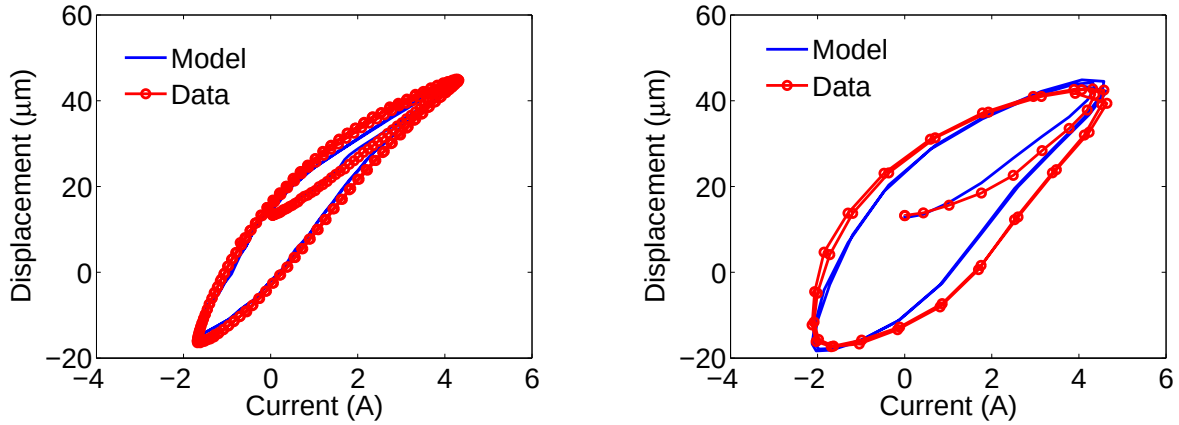

Figure 3: Rate-dependent constitutive data and comparison to the homogenized energy model described in Section 3. The model was fit to experiments at (a) 100 Hz and (b) 500 Hz.

4. Control Design

The nonlinear optimal control design is based on a previous numerical analysis for vibration control and tracking control [3,4,15]. The nonlinear control design is briefly summarized and experimental results are given. To illustrate the effectiveness of the nonlinear control design, the new method is compared to Proportional-Integral control.

Previous numerical analysis focused on identifying the nonlinear magnetic field input required for minimizing vibration or tracking a reference signal when nonlinear and hysteretic magnetostrictive material behavior is present. Here, the nonlinear voltage control input must be determined. The inclusion of the voltage-current dynamics presented in Section 3.3 is discussed in this section to illustrate how the open loop nonlinear voltage control signal is implemented experimentally.

4.1 Proportional Integral Control Design

The PI controller was designed by identifying the open loop transfer function of the amplifier-actuator system in the near linear regime. The transfer function is defined by a voltage input and the magnetostrictive actuator tip displacement. Open loop characterization was measured using a swept sine voltage input from the DS1104 controller board where the output was the rod tip displacement. More details can be found in [13].

The PI controller was designed using the form

$$D(s) = K_P \frac{s + K_I/K_P}{s}. \tag{21}$$

where K_P is the proportional gain and K_I is the integral gain. The control gains were chosen to enhance stability and bandwidth based on the open loop frequency response characterization. Gains of $K_P = 2 \times 10^{-2}$ V/ppm and $K_P/K_I = 30$ s were chosen. The open loop controller-amplifier-actuator transfer function was measured using a swept sine controller input to quantify the phase margin as 45^o and the gain margin as 2, see [13]. The resulting closed loop bandwidth for PI control is 1140 Hz.

4.2 Nonlinear Optimal Tracking Control Design

We summarize here the formulation of a finite-dimensional nonlinear optimal tracking control design where an open loop control signal is computed off-line.

Optimal tracking control employs a cost functional to determine the optimal control input. The cost functional

$$\overline{J} = \frac{1}{2}(\mathbf{C}\mathbf{x}(t_f) - r(t_f))^T P(\mathbf{C}\mathbf{x}(t_f) - r(t_f)) + \int_{t_0}^{t_f} \left[\mathcal{H} - \lambda^T(t)\dot{\mathbf{x}}(t)\right] dt \tag{22}$$

penalizes the control input and the error between the Terfenol-D actuator displacement and the prescribed displacement where P penalizes large terminal values on the tracking error, $\mathcal{H}$ is the Hamiltonian, and $\lambda(t)$ is a set of Lagrange multipliers. The Hamiltonian is

$$\begin{aligned} \mathcal{H} &= \frac{1}{2}\left[(\mathbf{C}\mathbf{x}(t) - r(t))^T Q(\mathbf{C}\mathbf{x}(t) - r(t)) + u^T(t)Ru(t)\right] \\ &\quad +\lambda^T\left[\mathbf{A}\mathbf{x}(t) + [\mathbf{B}(u)](t) + \mathbf{G}(t)\right] \end{aligned} \tag{23}$$

where penalties on the tracking error and the control input are given by the variables Q and R, respectively.

The minimum of the cost functional in (22) is determined under the constraint of the differential equation given by (12). By employing Lagrange multipliers an unconstrained minimization problem is constructed where the stationary condition for the Hamiltonian yields the adjoint relation [16, 17]

$$\dot{\lambda}(t) = -\mathbf{A}^{\mathbf{T}}\lambda(t) - \mathbf{C}^{\mathbf{T}}Q\mathbf{C}\mathbf{x}(t) + \mathbf{C}^{\mathbf{T}}Qr(t) \tag{24}$$

and optimal control input

$$u^*(t) = -R^{-1}\left(\frac{\partial \mathbf{B}(u)}{\partial u}\right)^T \lambda(t). \tag{25}$$

The resulting optimality system is

$$\begin{aligned} &\begin{bmatrix} \dot{\mathbf{x}}(t) \\ \dot{\lambda}(t) \end{bmatrix} = \begin{bmatrix} \mathbf{A}\mathbf{x}(t) + [\mathbf{B}(u^*)](t) + \mathbf{G}(t) \\ -\mathbf{A}^{\mathbf{T}}\lambda(t) - \mathbf{C}^{\mathbf{T}}Q\mathbf{C}\mathbf{x}(t) + \mathbf{C}^{\mathbf{T}}Qr(t) \end{bmatrix} \\ &\mathbf{x}(t_0) = \mathbf{x_0} \\ &\lambda(t_f) = \mathbf{C}^{\mathbf{T}}P\left(\mathbf{C}\mathbf{x}(t_f) - r(t_f)\right). \end{aligned} \tag{26}$$

The force determined from (9) is included in the input operator $[\mathbf{B}(u^*)](t)$ which directly includes the rate-dependent nonlinear and hysteretic $H - M$ behavior within the control design. This dynamic system results in a two-point boundary value problem which precludes an efficient Riccati formulation due to the nonlinear nature of the input operator. This system of equations and the boundary conditions are solved using a quasi-Newton method to determine the nonlinear magnetic field input; see [3] for more details.

This control design is formulated to quantify the nonlinear magnetic field applied to the magnetostrictive actuator. For experimental implementation the corresponding voltage control must be determined. The relation used to numerically determine the voltage control from the optimal magnetic field input in (25) and the current-field relation in (14). The nonlinear voltage-current relation in (13) is solved using a central difference temporal discretization

$$V_k = \frac{1}{2}\left(L(M_k) + L(M_{k+1})\right)\frac{i_{k+1} + i_k}{\Delta t} + \frac{1}{2}R\left(i_{k+1} + i_k\right) \tag{27}$$

where a temporal step size Δt is employed giving a discretization in time defined by $t_k = k\Delta t$. The voltage solved in (27) is the nonlinear open loop control input used in the experiments.

5. Tracking Control Experimental Results

The performance characteristics of the PI controller and open loop nonlinear optimal control design is given to illustrate operating regimes where the nonlinear controller provides enhanced tracking control. The commanded reference input to the controller was a sinusoidal signal. A 30 μm reference signal amplitude was used to introduce significant nonlinearities as previously illustrated in Figure 3. The results from control experiments for frequencies 100, 500, 700, and 1000 Hz are illustrated in Figure 4 for both control designs.

Comparable performance was achieved between the PI controller and the nonlinear optimal control design for the 100 Hz reference displacement. Marginal differences in tracking control became apparent at 500 Hz. A phase lag occurs due to the hysteresis as the frequency increases above 500 Hz. As the reference displacement frequency approaches the bandwidth of the PI controller, the amplification in the closed loop system degrades tracking control; see Figure 4(b)-(d). It should also be noted that minor errors in drift occur at 1000 Hz using nonlinear open loop control, but this error can be corrected by including perturbation feedback, see [3, 4, 18] for details.

6. Concluding Remarks

The incorporation of the homogenized energy model in the nonlinear optimal control design was shown to significantly improve tracking control at frequencies up to at least 1 kHz. Reasonable robustness in model predictions was illustrated by fitting a single set of rate-dependent material parameters to data between 100

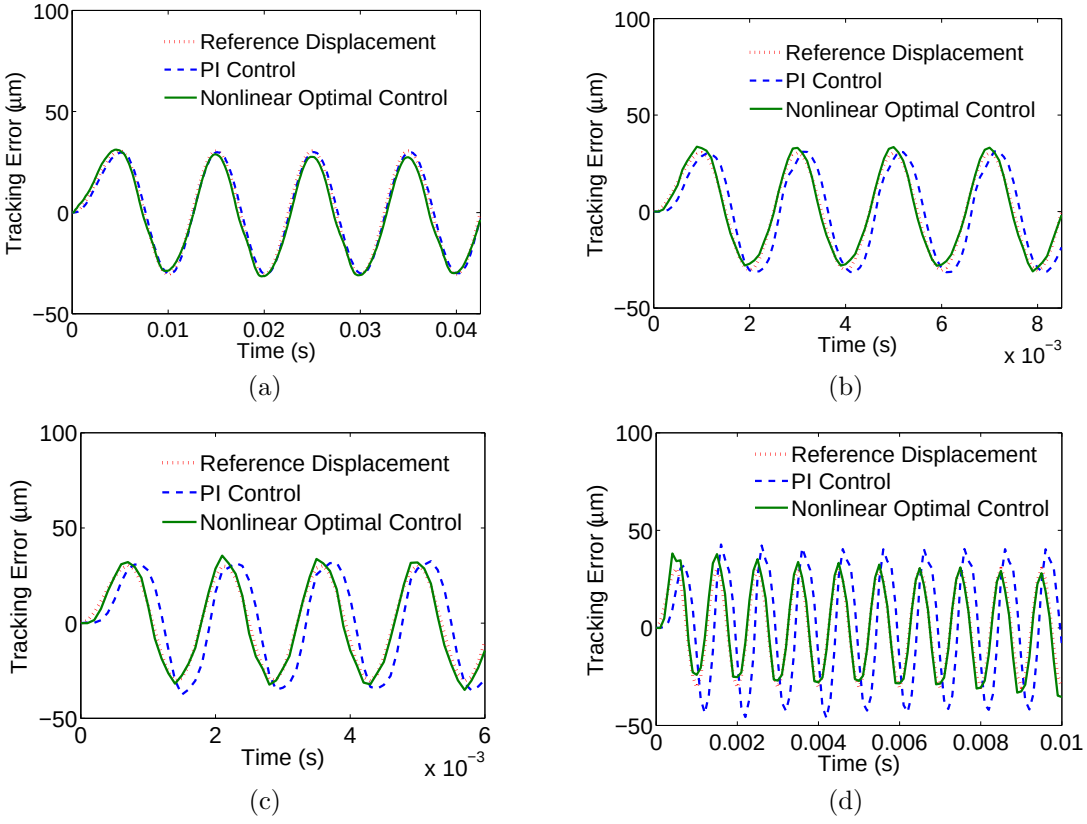

Figure 4: Comparison of the tracking control performance using PI control, nonlinear open loop optimal control and nonlinear open loop optimal control. The frequencies tested include (a) 100 Hz, (b) 500 Hz, (c) 700 Hz, (d) and 1000 Hz.

and 500 Hz which was then used in controlling the Terfenol-D actuator up to 1 kHz. As previously noted, only current vs. displacement data was measured which required estimating the current vs. magnetization hysteresis loops. Since the induction of the magnetostrictive actuator was not measured, uncertainty in estimating certain rate-dependent model parameters occurred. While this limits achieving an accurate model prediction of both displacement and magnetization, it illustrates the ability to implement the model-based control design on magnetostrictive actuators in situations where the magnetization is not measurable but only displacement tracking is desired.

The nonlinear optimal control design has focused on applications where the reference displacement is known in advance and precise control is desired at relatively high speed. For these applications, the nonlinear control input can be computed off-line and then implemented in real-time control applications. Although the numerical procedure requires convergence of a nonlinear two-point boundary value problem, once the numerical procedure is developed, the control input for most reference signals (within physical limitations) can be quantified. This approach provides an alternative to nonlinear inverse compensator designs which depend on the ability to invert the constitutive model efficiently in real-time.

The PI controller provided good tracking control at 100 Hz and performance degradation began to occur at 500 Hz. The effects of nonlinearities and hysteresis previously illustrated in Figure 3 become significant at higher frequencies which limits precise displacement control. Conversely, when the nonlinear optimal control design is implemented, the tracking errors are reduced and good performance is achieved up to at least 1000 Hz.

Acknowledgments

The authors gratefully acknowledge support from the Air Force Office of Scientific Research through the grant AFOSR-FA9550-04-1-0203. The authors also wish to acknowledge Dr. Julie Slaughter of Etrema Products, Inc., for supplying the Terfenol-D material used in this study.

References

[1] R. O'Handley, S. Murray, M. Marioni, H. Nembach, and S. Allen, "Phenomenology and giant magnetic-field-induced strain in ferromagnetic shape-memory meterials," *J. Appl. Phys.*, vol. 87, no. 9, pp. 4712–4717, 2000.

[2] X. Tan and J. Baras, "Modeling and control of hysteresis in magnetostrictive actuators," *Automatica*, vol. 40, pp. 1469–1480, 2004.

[3] R. Smith, "A nonlinear optimal control method for magnetostrictive actuators," *J. Intell. Mater. Syst. Struct.*, vol. 9, no. 6, pp. 468–486, 1995.

[4] W. Oates and R. Smith, "Nonlinear optimal control techniques for vibration attenuation using nonlinear magnetostrictive actuators," *to appear in the J. Intell. Mater. Sys. Struct.*, 2007.

[5] R. Smith, M. Dapino, T. Braun, and A. Mortensen, "A homogenized energy framework for ferromagnetic hysteresis," *IEEE Trans. Mag.*, vol. 42, no. 7, pp. 1747–1769, 1995.

[6] R. Smith, S. Seelecke, M. Dapino, and Z. Ounaies, "A unified framework for modeling hysteresis in ferroic materials," *J. Mech. Phys. Solids*, vol. 54, no. 1, pp. 46–55, 2005.

[7] R. Smith, M. Dapino, and S. Seelecke, "A free energy model for hysteresis in magnetostrictive transducers," *J. Appl. Phys.*, vol. 93, no. 1, pp. 458–466, 2003.

[8] R. Smith, S. Seelecke, Z. Ounaies, and J. Smith, "A free energy model for hysteresis in ferroelectric materials," *J. Intell. Mater. Syst. Struct.*, vol. 14, no. 11, pp. 719–739, 2003.

[9] R. Smith, A. Hatch, B. Mukherjee, and S. Liu, "A homogenized energy model for hysteresis in ferroelectric materials: General density formulations," *J. Intell. Mater. Syst. Struct.*, vol. 16, no. 9, pp. 713–732, 2005.

[10] R. Smith, *Smart Material Systems: Model Development*. Philadelphia, PA: SIAM, 2005.

[11] T. Braun and R. Smith, "Efficient implementation algorithms for homogenized energy models," *Continuum Mech. Thermodyn.*, vol. 18, no. 3-4, pp. 137–155, 2006.

[12] M. Dapino, R. Smith, and A. Flatau, "A structural strain model for magnetostrictive transducers," *IEEE T. Magn.*, vol. 36, no. 3, pp. 545–556, 2000.

[13] W. Oates, P. Evans, R. Smith, and M. Dapino, "Experimental implementation of a hybrid nonlinear control design for magnetostrictive transducers," *submitted to IEEE T. Contr. Syst. T.*

[14] R. Serway, *Physics For Scientists and Engineers*. Saunders College Publishing, 1990.

[15] W. Oates and R. Smith, "Nonlinear perturbation control for magnetic transducers," *accepted to the IEEE Conference on Decision and Control*, 2007.

[16] A. Bryson and Y.-C. Ho, *Applied Optimal Control*. Waltham, MA: Blasidell Publishing Company, 1969.

[17] F. Lewis and V. Syrmos, *Optimal Control*. New York, NY: John Wiley and Sons, 1995.

[18] W. Oates and R. Smith, "Optimal tracking using magnetostricive actuators operating in the nonlinear and hysteretic regime," *submitted to J. Dyn. Syst.-T. ASME*.